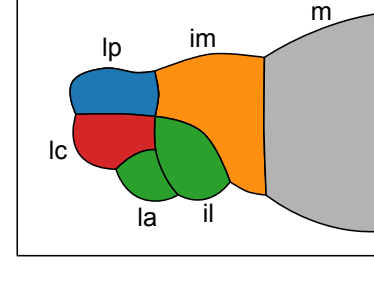
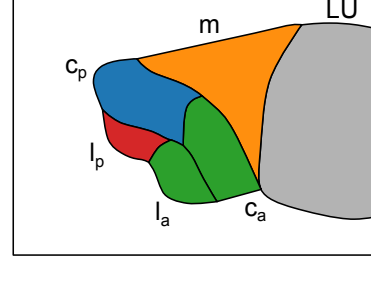


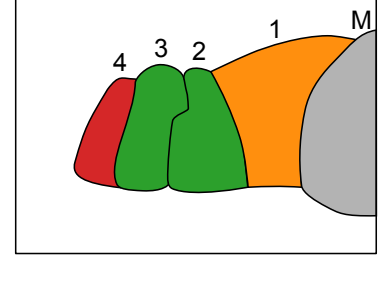
d_i
Omoto and Keles et al. 2017



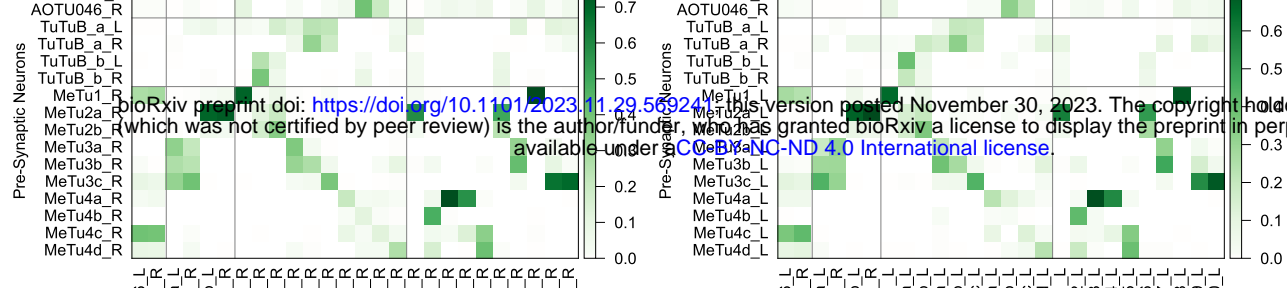
d_ii
Timaeus et al. 2020



d_iii
Tai et al. 2020



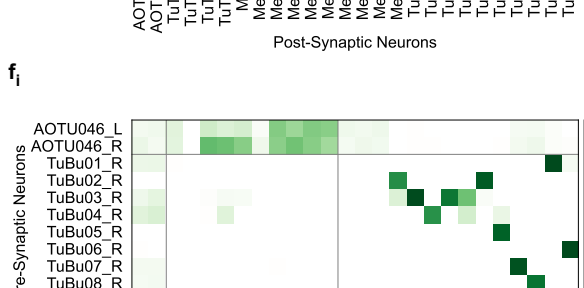
e_i



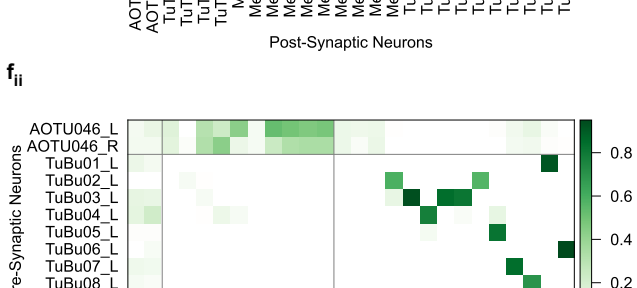
e_ii



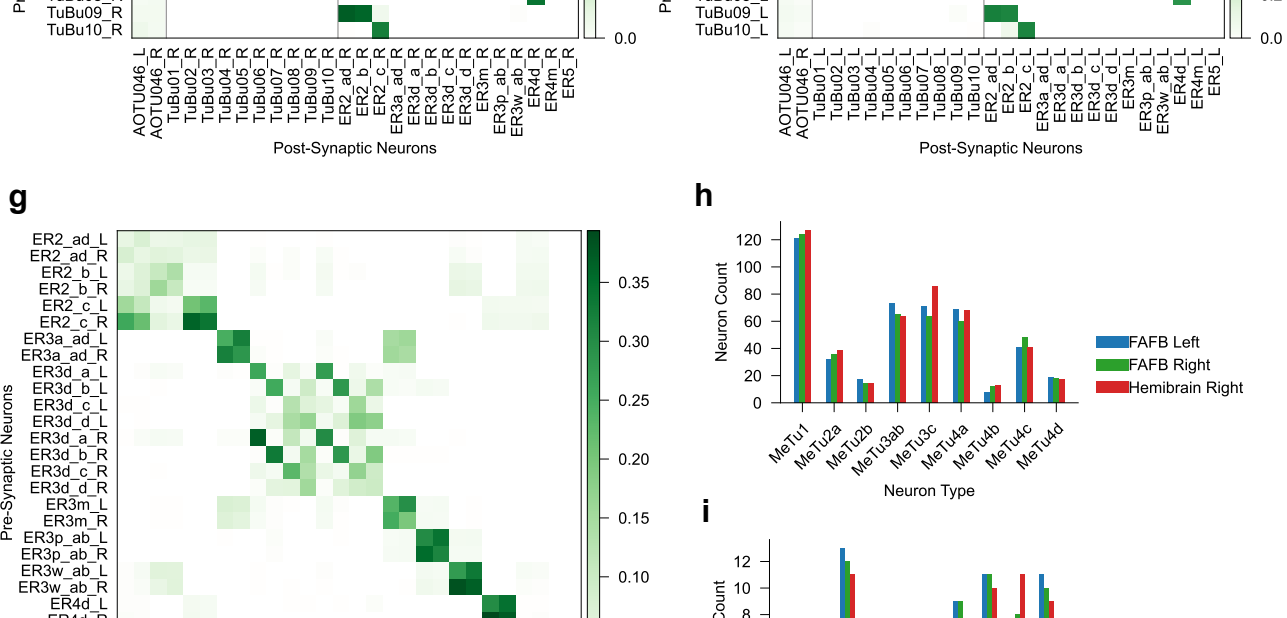
f_i



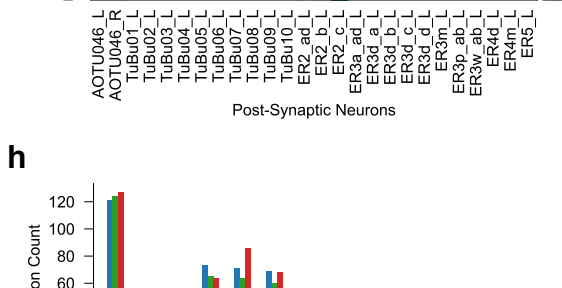
f_ii



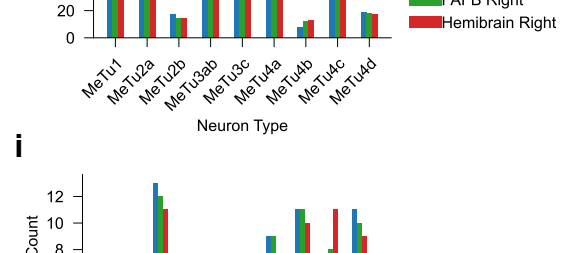
g



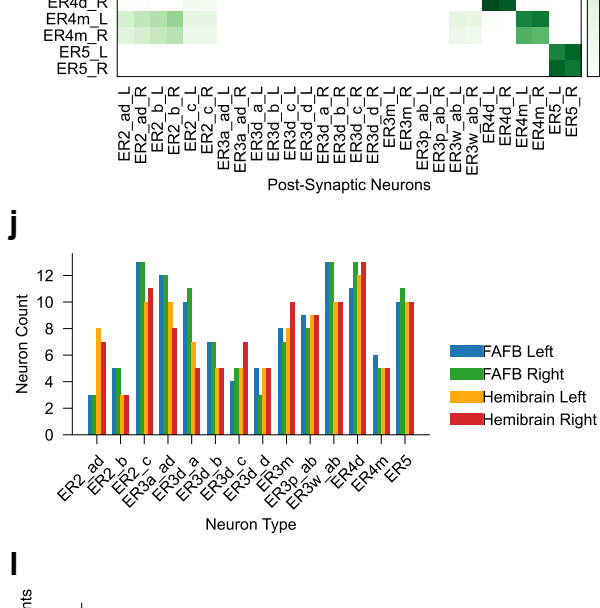
h



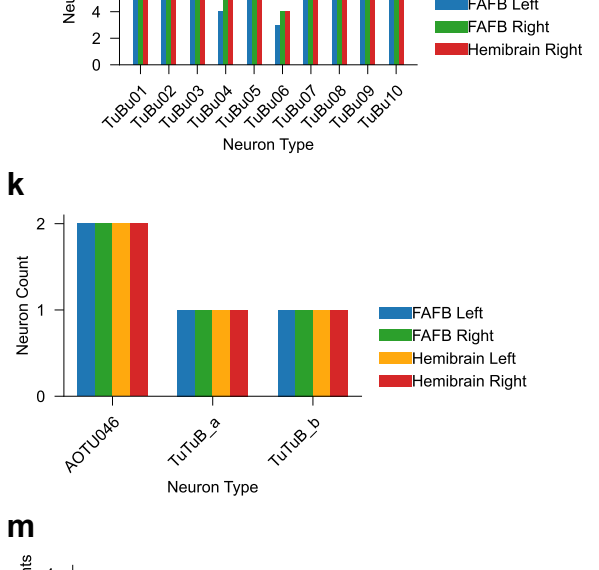
i



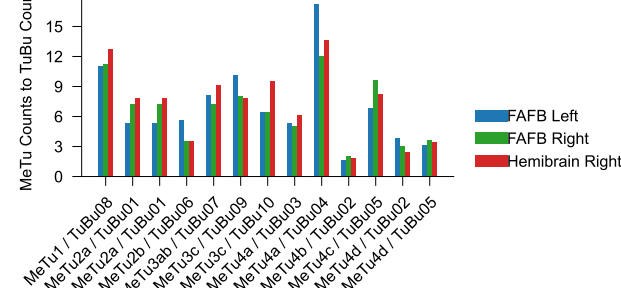
j



k



l



m

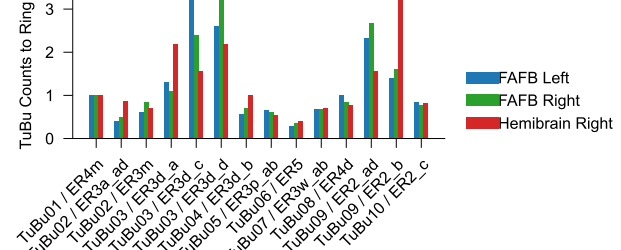


Fig. S1 | Methods of analysis of the AVP and AOTU_SU. **a**, Diagram of Flywire. Left: multiple stacked EM layers. Right: Image of the Flywire interface. **b**, Quality control through three rounds of proofreading among 113 MeTu neurons of the right hemisphere. The total number of edits per neuron per round (**b_i**) and the change in volume from before to after each proofreading round (**b_{ii}**). **C_{i-iii}**, EM data quality of the left and right optic lobe . (**c_i**) EM slice of the fly brain, note the partially detached lamina (arrow) on the left optic lobe. (**c_{ii}**) and (**c_{iii}**) MeTu1 neurons of the right and left optic lobe respectively viewed from the dorsal side , note the uneven image alignment on the posterior side (arrow) of the left optic lobe (**c_{iii}**). **d_{i-iii}**, Comparison of different illustrations of the AOTUsu subregion [35, 41, 56]. **e_{i-ii}**, Synaptic weight matrix of bihemispheric neuron types and MeTu subtypes to themselves and TuBu types on the right (**e_i**) and left (**e_{ii}**) hemisphere. **f_{i-ii}**, Synaptic weight matrix of bihemispheric neuron types and TuBu types to themselves and Ring neurons, on the right (**f_i**) and left (**f_{ii}**) hemisphere. **g**, Synaptic weight matrix of all visual Ring neuron subtypes. **h-k**, Comparing neuron counts between both hemispheres in the FAFB and applicable hemispheres in the hemibrain datasets, of MeTu (**h**), TuBu (**i**), Ring (**j**), and bihemispheric (**k**) neurons. Note the difference between FAFB and hemibrain data. For example, in FAFB, there are only six ER2_a/d neurons (3/side) while the hemibrain has 15 of these neurons (eight on the left, seven on the right) (**j**). Because there were no verifiable differences among these neurons, we categorized them as a single group. Similarly, although the total number of ER3a_ad neurons was similar between FAFB and hemibrain data, we were unable to identify distinct features to differentiate ER3a_a and ER3a_d in FAFB (**j**). Thus, we combined them into a single group as well. We did the same with ER3p_ab and ER3w_ab, as potential subtypes were similarly indistinguishable (**j**). **l-m**, Comparing the ratios of MeTu to TuBu (**l**) and TuBu to Ring (**m**) between both datasets in applicable hemispheres.

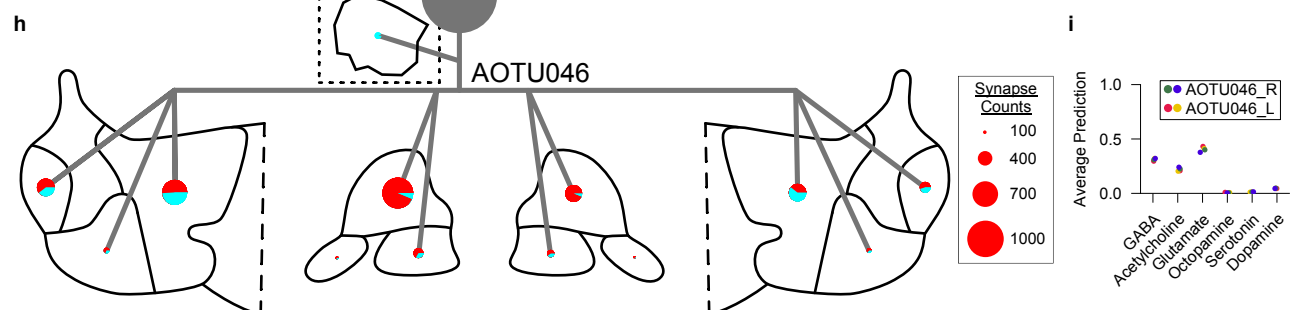
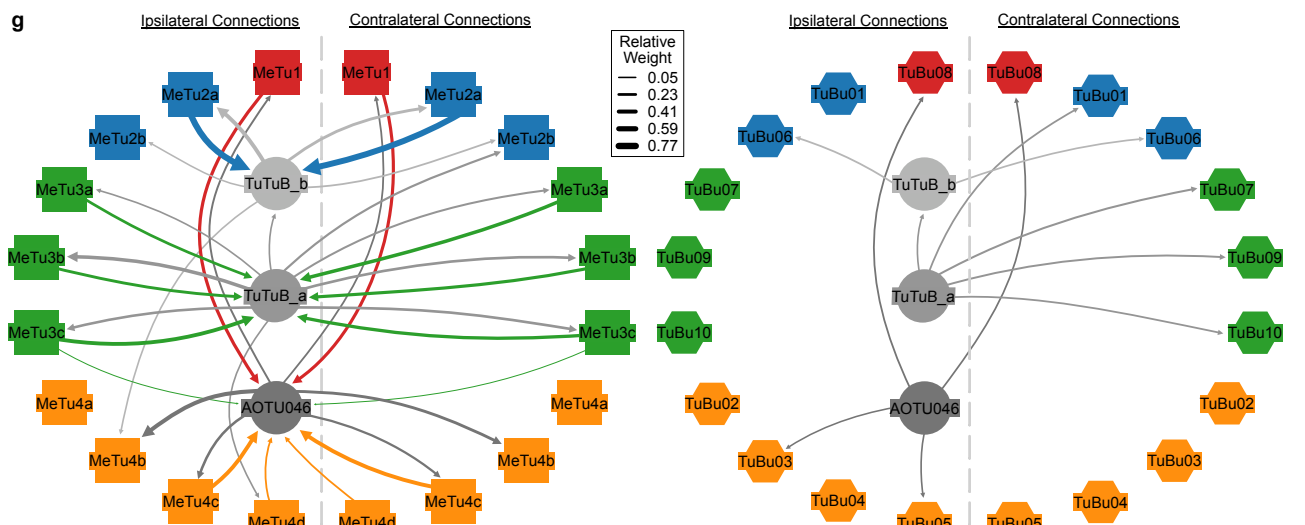
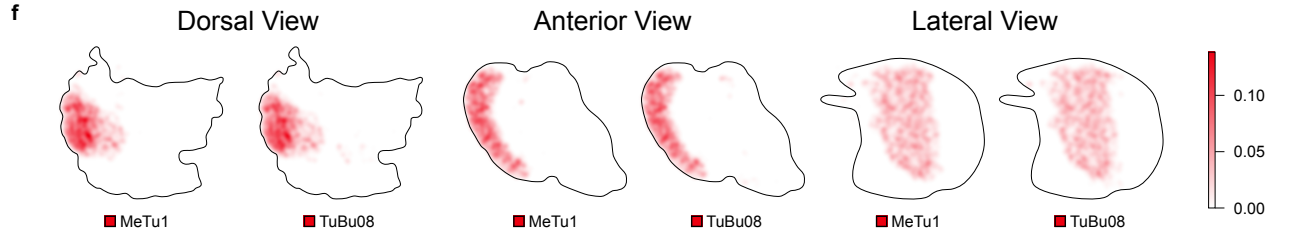
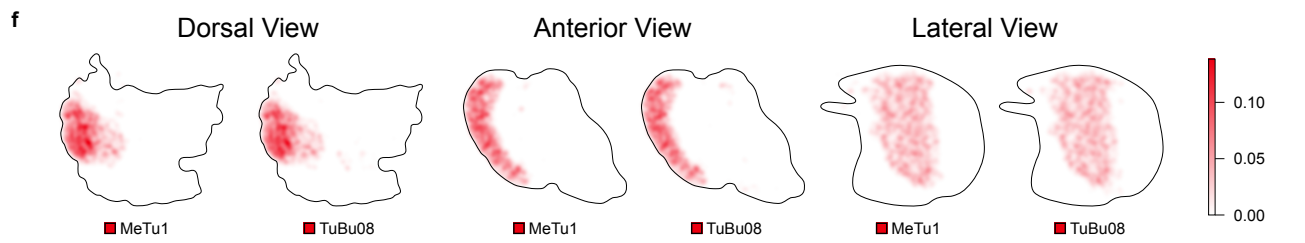
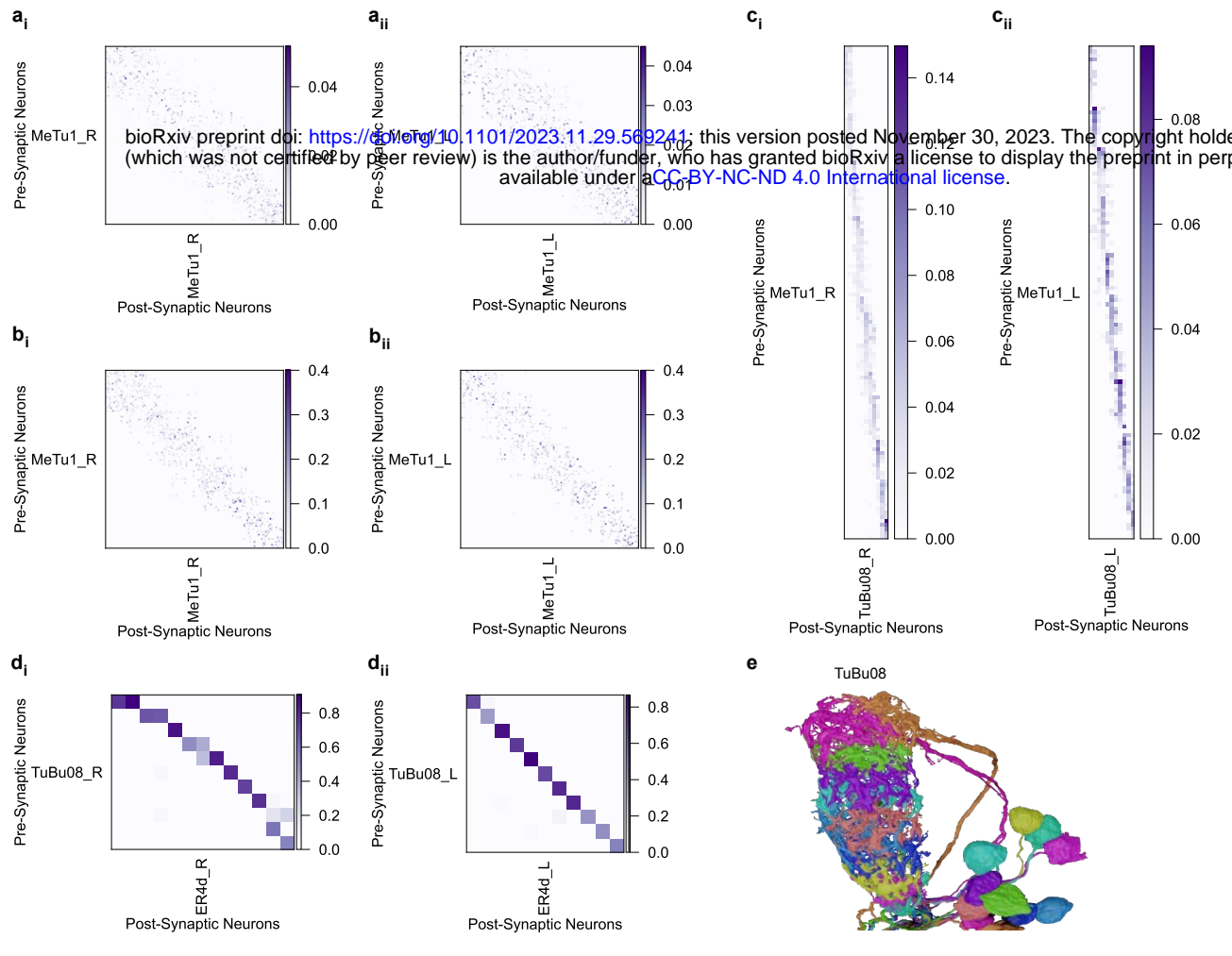


Fig. S2 | MeTu1 Pathway Connectivity. **a_{i-ii}**, Synaptic weight matrices of MeTu1 interconnectivity within the medulla in the right (**a_i**) and left (**a_{ii}**) hemisphere. **b_{i-ii}**, Synaptic weight matrices of MeTu1 interconnectivity within the AOTU in the right (**b_i**) and left (**b_{ii}**) hemisphere. **c_{i-ii}**, Synaptic weight matrices of MeTu1 to TuBu08 in the AOTU in the right (**c_i**) and left (**c_{ii}**) hemisphere. **d_{i-ii}**, Synaptic weight matrices of TuBu08 to ER4d in the Bulb in the right (**d_i**) and left (**d_{ii}**) hemisphere. **e**, All TuBu08 neurons of AOTUsu in the right hemisphere from the lateral perspective. Viewed from the anterior side, AOTUsu_PL is curved like a bow. Perpendicular cross sections through this domain appear elliptical, tapering along the ventral direction. **f**, Synapse density maps of connections between MeTu1 and TuBu08 neurons in the AOTU_SU from the dorsal, anterior, and lateral perspectives. All perspectives have been rotated 30° with respect to the anterior-posterior axis, and synapse densities were blurred with a Gaussian filter with a sigma value of 10. **g**, Left: Synaptic weight between bihemispheric neuron types and MeTu subtypes on the ipsilateral (left) and contralateral (right) sides. Right: Similar to the left, Synaptic weight between bihemispheric neuron types and TuBu types. MeTu2a receives strong synaptic inputs from TuTuB_b on both sides, but none from TuTuB_a. It also reciprocally provides strong inputs to TuTuB_b on both sides, but only very weak input to TuTuB_a. **h**, Diagram of an AOTU046 neuron. AOTU046 neurons innervates AOTUsu_M, where they send sparse axons along the anterior/posterior-lateral face and extend boutons toward the posterior-medial triangle vertex at only a single latitude halfway down the dorsal-ventral axis. Pie charts are the ratio of presynaptic (red) to postsynaptic (cyan) connections to AVP neurons in the AOTU and Bulb regions, and connections to all neurons in the SPS. The SPS depicted in a cutout. Pie chart sizes are based on the relative number of connections (legend on the right). **i**, Average neurotransmitter prediction score over all synapses in each AOTU046 neuron for each type of neurotransmitter.

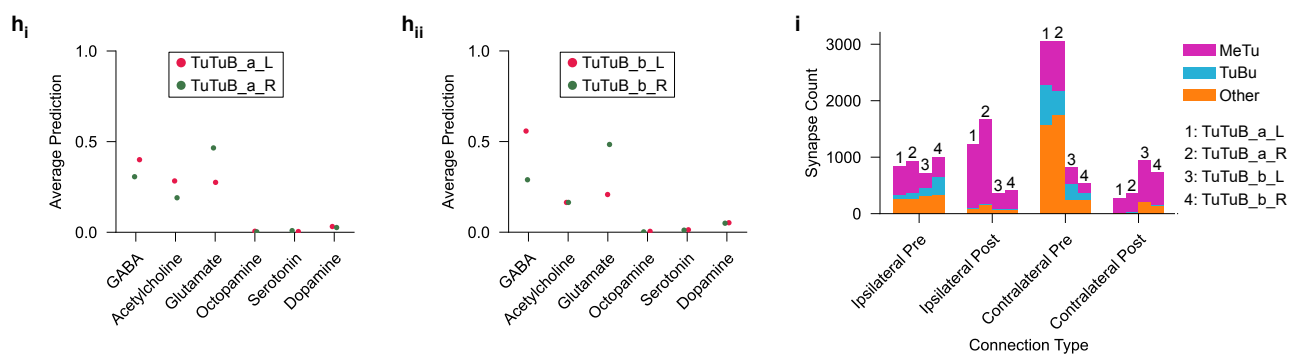
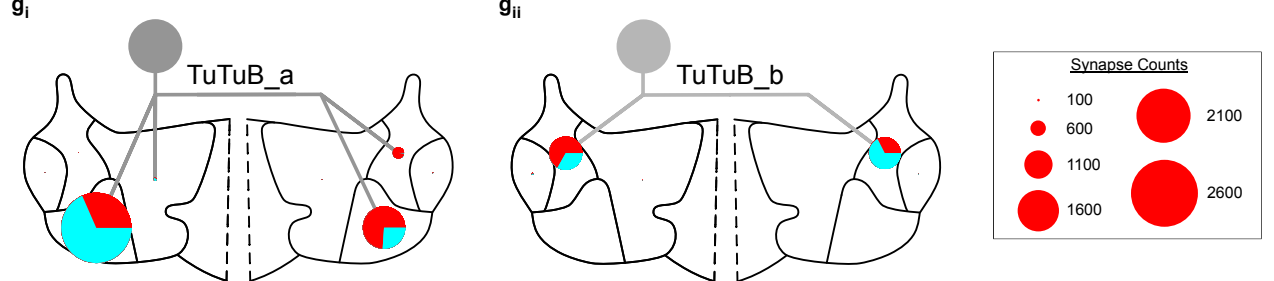
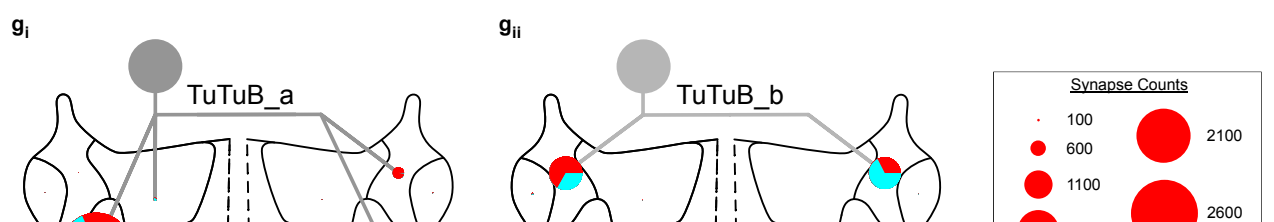
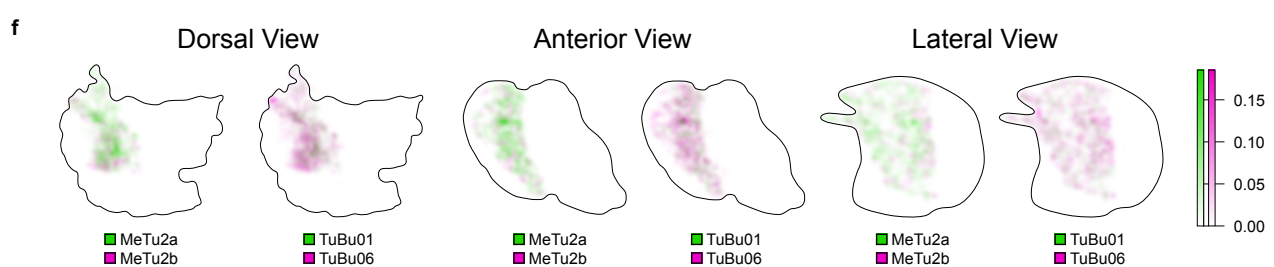
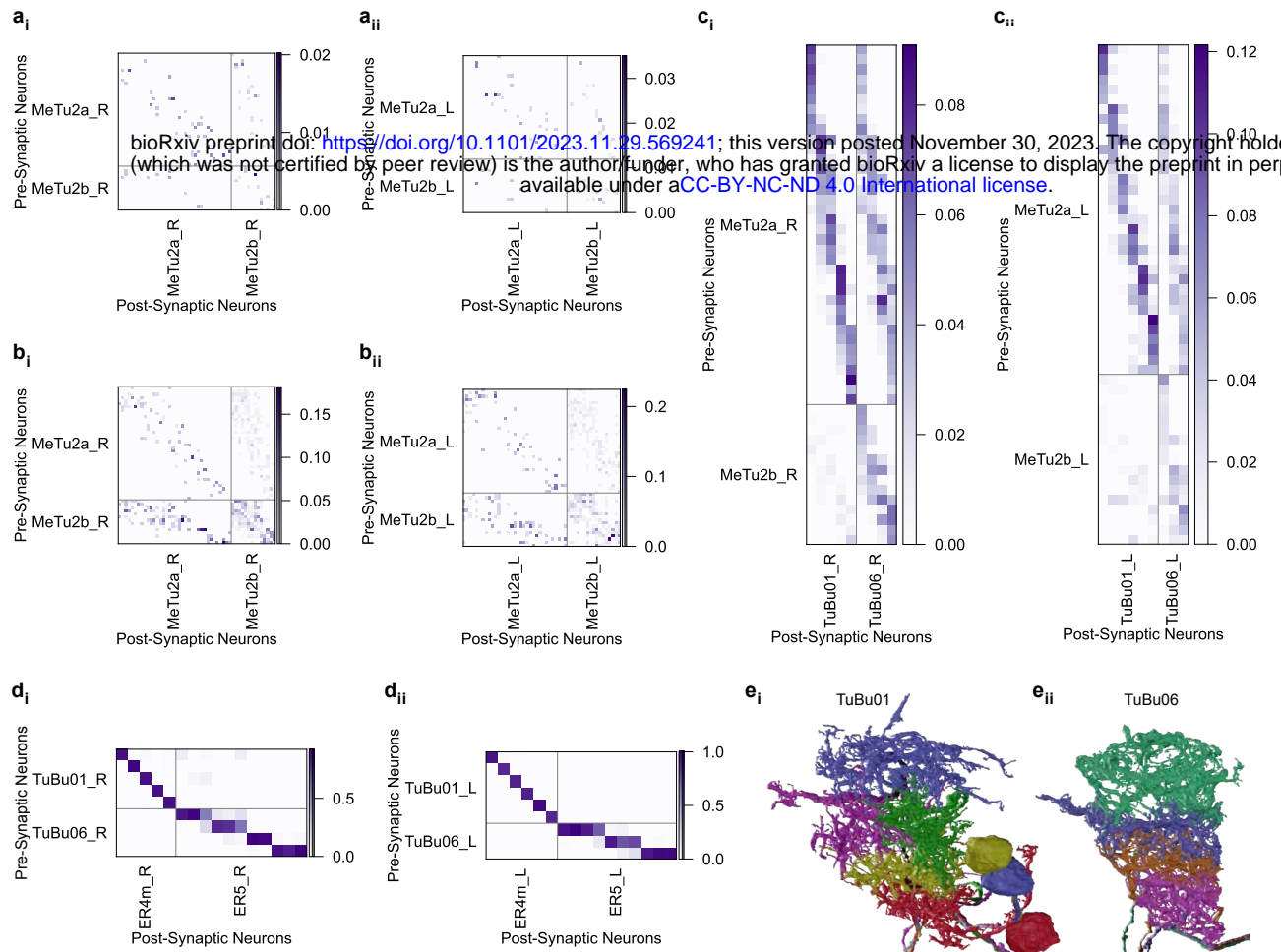


Fig. S3 | MeTu2 Pathway Connectivity. **a_{i-ii}**, Synaptic weight matrices of MeTu2 interconnectivity within the medulla in the right (**a_i**) and left (**a_{ii}**) hemisphere. **b_{i-ii}**, Synaptic weight matrices of MeTu2 interconnectivity within the AOTU of the right (**b_i**) and left (**b_{ii}**) hemisphere. **c_{i-ii}**, Synaptic weight matrices of MeTu2 to TuBu1 and TuBu06 in the AOTU in the right (**c_i**) and left (**c_{ii}**) hemisphere. **d_{i-ii}**, Synaptic weight matrices of TuBu01 and TuBu06 to relevant Ring neurons in the bulb in the right (**d_i**) and left (**d_{ii}**) hemisphere. **e_{i-ii}**, All TuBu01 (**e_i**) and TuBu06 (**e_{ii}**) neurons from the lateral perspective in the AOTUsu. The cross-section of AOTUsu_PC is curved and slightly wraps around the AOTUsu_PL. Like the AOTUsu_PL, the area becomes thinner towards the ventral side. **f**, Synapse density maps of connections between MeTu2 and TuBu1 and TuBu06 neurons in the AOTU_SU from the dorsal, anterior, and lateral perspectives. All perspectives have been rotated 30° with respect to the anterior-posterior axis, and synapse densities were blurred with a Gaussian filter with a sigma value of 10. The distribution of presynaptic boutons of each MeTu2 neuron extends across the entire anterior-posterior axis of AOTUsu_PC, but the distribution is restricted along the dorsal-ventral axis. **g_{i-ii}**, Diagrams of TuBuB_a (**g_i**) and TuBuB_b (**g_{ii}**) neurons. Boutons of TuTuB_a [28] sparsely protrude into the posterior central area only on the opposite side of the soma, while both axons and dendrites of TuTuB_b neurons [ref] innervate the entire AOTUsu_PC. Pie charts are the ratio of presynaptic (red) to postsynaptic (cyan) connections to AVP neurons in the AOTU and Bulb. Pie chart sizes are based on the relative amount of connections (legend on the right). **h_{i-ii}**, The average neurotransmitter prediction score over all synapses in each TuTuB_a (**h_i**) or TuTuB_b (**h_{ii}**) neuron for each type of neurotransmitter. **i**, Number of synapses of each TuTuB neuron between the ipsilateral and contralateral hemisphere, based on the type of neuron it is connected to.

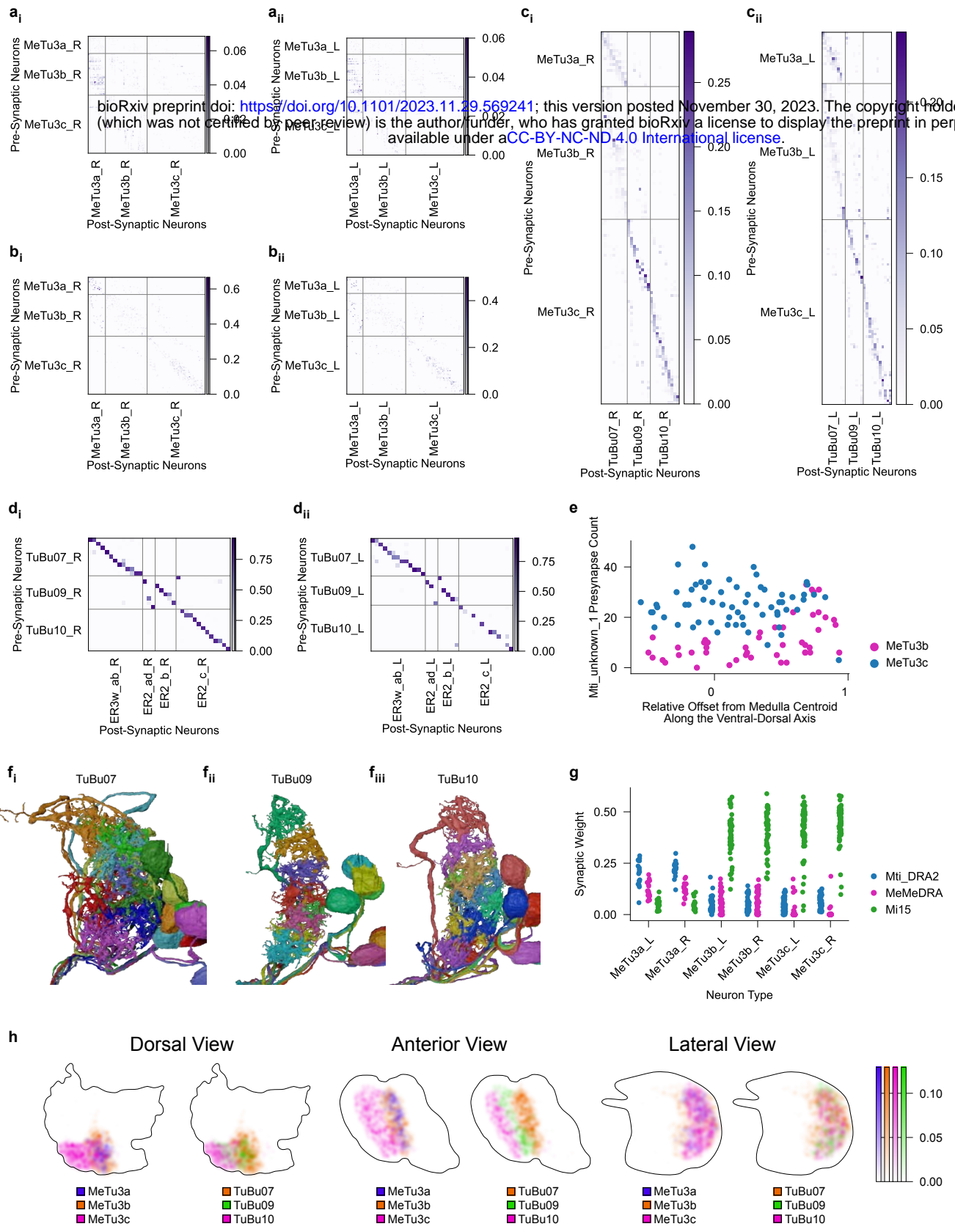


Fig. S4 | MeTu3 Pathway Connectivity. **a_{i-ii}**, Synaptic weight matrices of MeTu3 interconnectivity within the medulla in the right (**a_i**) and left (**a_{ii}**) hemisphere. **b_{i-ii}**, Synaptic weight matrices of MeTu3 interconnectivity within the AOTU in the right (**b_i**) and left (**b_{ii}**) hemisphere. **c_{i-ii}**, Synaptic weight matrices of MeTu3 to TuBu_A in the AOTU in the right (**c_i**) and left (**c_{ii}**) hemisphere. **d_{i-ii}**, Synaptic weight matrices of TuBu_A to relevant Ring neurons in the bulb in the right (**d_i**) and left (**d_{ii}**) hemisphere. **e**, Number of synapses from Mti_unknown_1 onto MeTu3b (pink) and MeTu3c (blue) neurons in the right hemisphere as a function of their relative position along the dorsal-ventral axis. 0 on the x-axis refers to the center of the Medulla, while positive values are more dorsal and negative values are more ventral. **f_{i-iii}**, All TuBu07 (**f_i**), TuBu09 (**f_{ii}**), and TuBu10 (**f_{iii}**) neurons of AOTUsu in the right hemisphere from the lateral perspective. The volume of AOTUsu_A is flat on the posterior and the medial sides and curves in a quarter-ellipse from the lateral edge to the anterior edge. **g**, Synaptic weight of upstream neurons to all neurons of the different subtypes of MeTu3. **h**, Synapse density maps of connections between MeTu3 and TuBu_A neurons in the AOTU_SU from the dorsal, anterior, and lateral perspectives. All perspectives have been rotated 30° with respect to the anterior-posterior axis, and synapse densities were blurred with a Gaussian filter with a sigma value of 10.

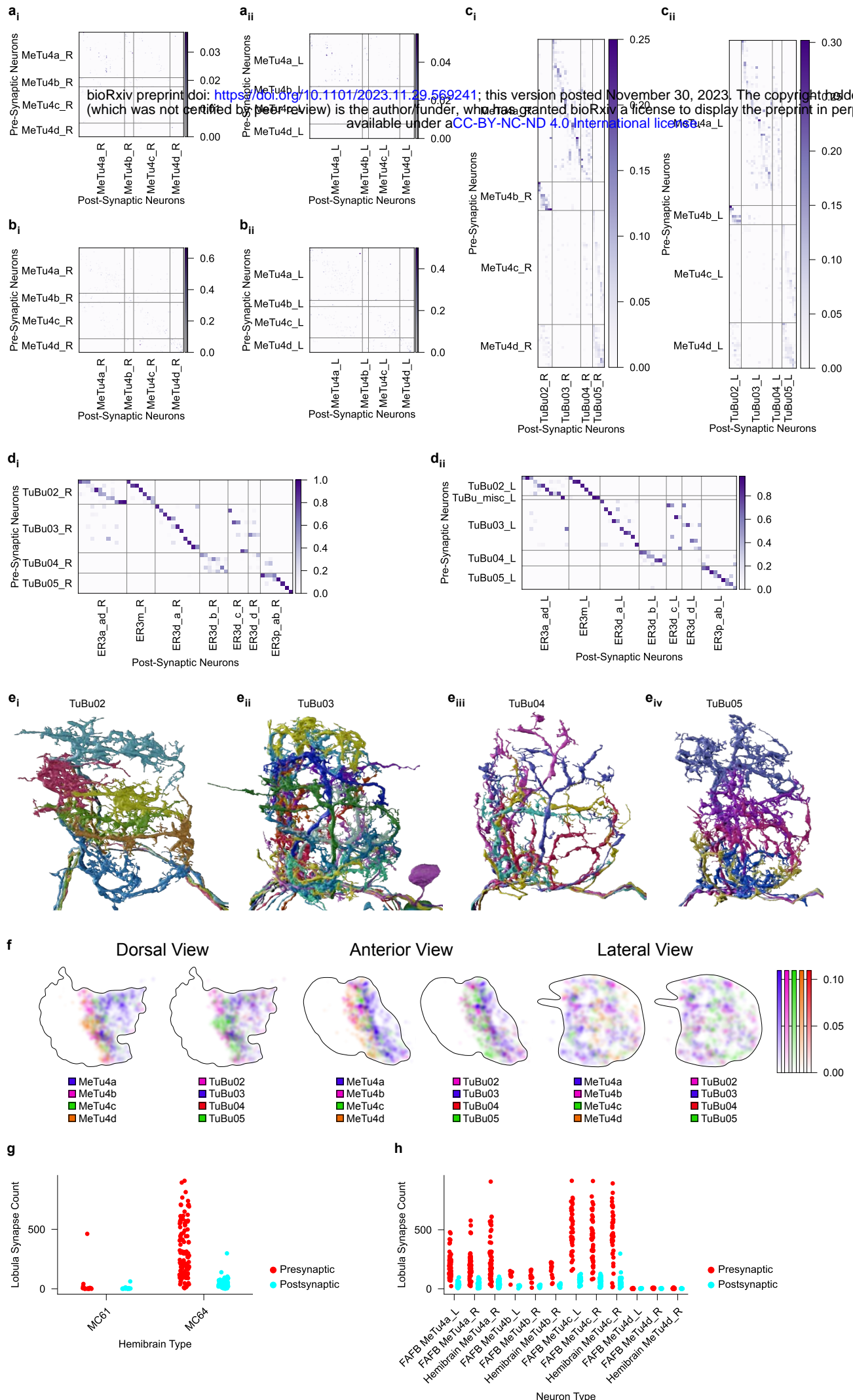


Fig. S5 | MeTu4 Pathway Connectivity. **a_{i-ii}**, Synaptic weight matrices of MeTu4 interconnectivity within the medulla in the right (**a_i**) and left (**a_{ii}**) hemisphere. **b_{i-ii}**, Synaptic weight matrices of MeTu4 interconnectivity within the AOTU in the right (**b_i**) and left (**b_{ii}**) hemisphere. **c_{i-ii}**, Synaptic weight matrices of MeTu4 to TuBu02/03/04/05in the AOTU in the right (**c_i**) and left (**c_{ii}**) hemisphere. **d_{i-ii}**, Synaptic weight matrices of TuBu TuBu02/03/04/05 to relevant Ring neurons in the bulb in the right (**d_i**) and left (**d_{ii}**) hemisphere. **e_{i-iv}**, All TuBu02 (**e_i**), TuBu03 (**e_{ii}**), TuBu04 (**e_{iii}**), and TuBu05 (**e_{iv}**) neurons of AOTUsu in the right hemisphere from the lateral perspective. The cross-section of AOTUsu_M appears right-triangle-shaped. One edge of the triangle is the boundary between AOTUsu_M and both AOTUsu_PC and AOTUsu_A, while the opposite vertex extends medially outward on the posterior side. Some MeTu and TuBu types cluster only along the region border, while others fill the entire triangle. **f**, Synapse density maps of connections between MeTu4 and TuBu02/03/04/05neurons in the AOTU_SU from the dorsal, anterior, and lateral perspectives. All perspectives have been rotated 30° with respect to the anterior-posterior axis, and synapse densities were blurred with a Gaussian filter with a sigma value of 10. **g**, Number of lobula presynapses (red) and postsynapses (cyan) of all MeTu4 neurons in the hemibrain dataset, sorted by whether they were previously classified as MC61 or MC64. MeTu4d neurons were generally classified as MC61, due to not having synapses in the lobula. **h**, Number of lobula presynapses (red) and postsynapses (cyan) of all MeTu4 neurons in both datasets after subclassification.

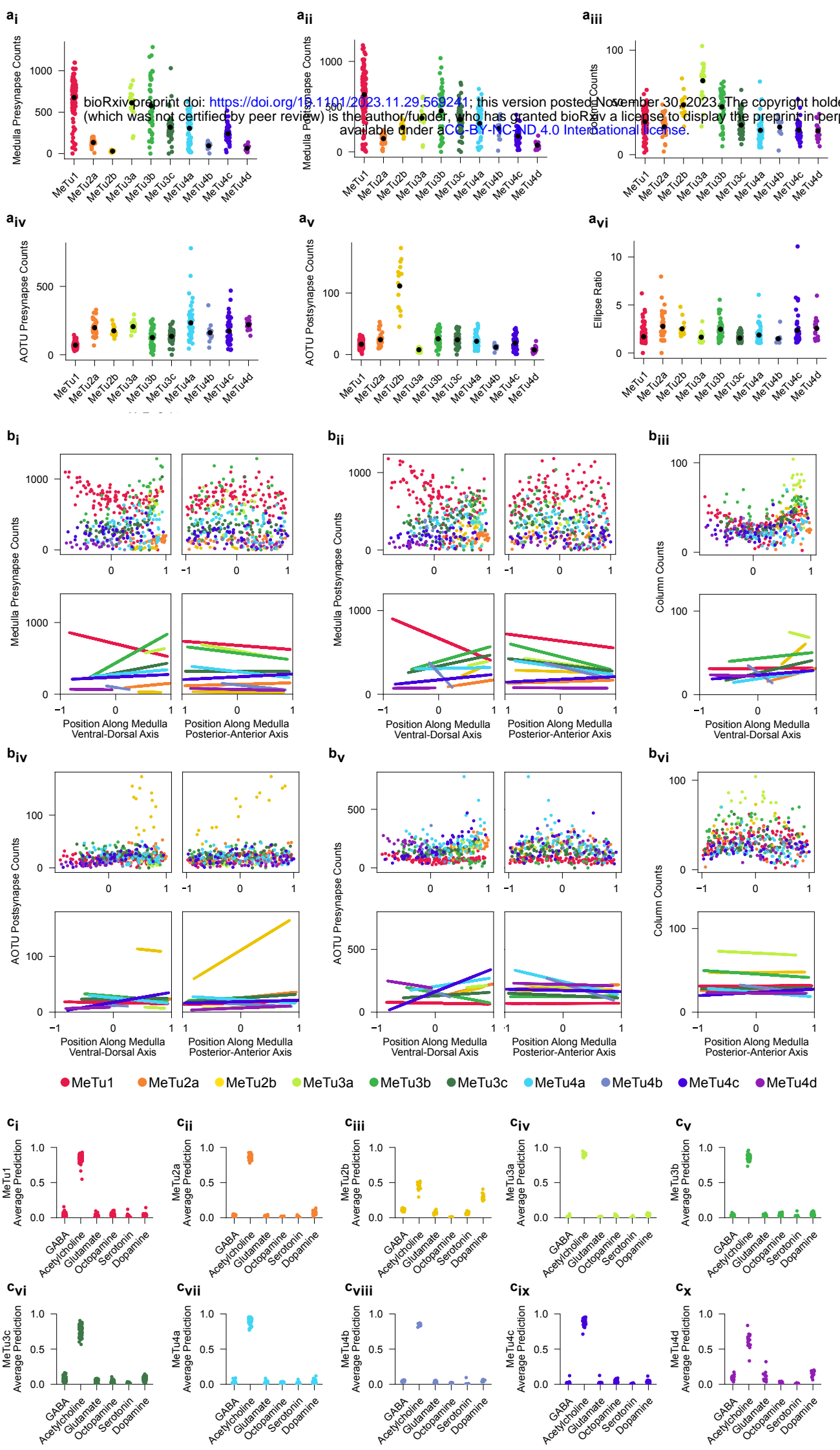


Fig. S6 | Comparisons Between MeTu Subtypes. **a**, Comparisons between all MeTu subtypes in the right hemisphere. Number of presynapses in the medulla (**a_i**), number of postsynapses in the medulla (**a_{ii}**), number of medulla columns that each neuron's dendritic span occupies (**a_{iii}**), number of presynapses in the AOTU (**a_{iv}**), number of postsynapses in the AOTU (**a_v**), and the ellipse ratio of the dendrites in the medulla (**a_{vi}**). **b**, Comparisons among all MeTu subtypes in the right hemisphere with respect to the ventral-dorsal axis (negative values are ventral, positive values are dorsal) and the posterior-anterior axis (negative values are posterior, positive values are anterior) of the medulla. Scatter plot of all MeTu neurons (top) and the line of best fit (bottom). The color legend is at the bottom of (**b**). **b_i**, Number of presynapses in the medulla as a function of the position along the ventral-dorsal axis (left) and posterior-anterior axis (right) of the medulla. **b_{ii}**, Number of postsynapses in the medulla as a function of the position along the ventral-dorsal axis (left) and posterior-anterior axis (right) of the medulla. **b_{iii}**, Number of medulla columns that each neuron's dendritic span occupies as a function of the position along the ventral-dorsal axis of the medulla. **b_{iv}**, Number of presynapses in the AOTU against the ventral-dorsal axis (left) and posterior-anterior axis (right) of the AOTU. **b_v**, Number of postsynapses in the AOTU against the ventral-dorsal axis (left) and posterior-anterior axis (right) of the AOTU. **b_{vi}**, Number of medulla columns that each neuron's dendritic span occupies as a function of the position along the posterior-anterior axis of the medulla. **c_{i-x}**, Average neurotransmitter prediction score over all synapses in each MeTu1/2a-b/3a-c/4a-d neuron respectively for each type of neurotransmitter. Note that the neurotransmitter of MeTu2b is not clearly predicted as cholinergic.

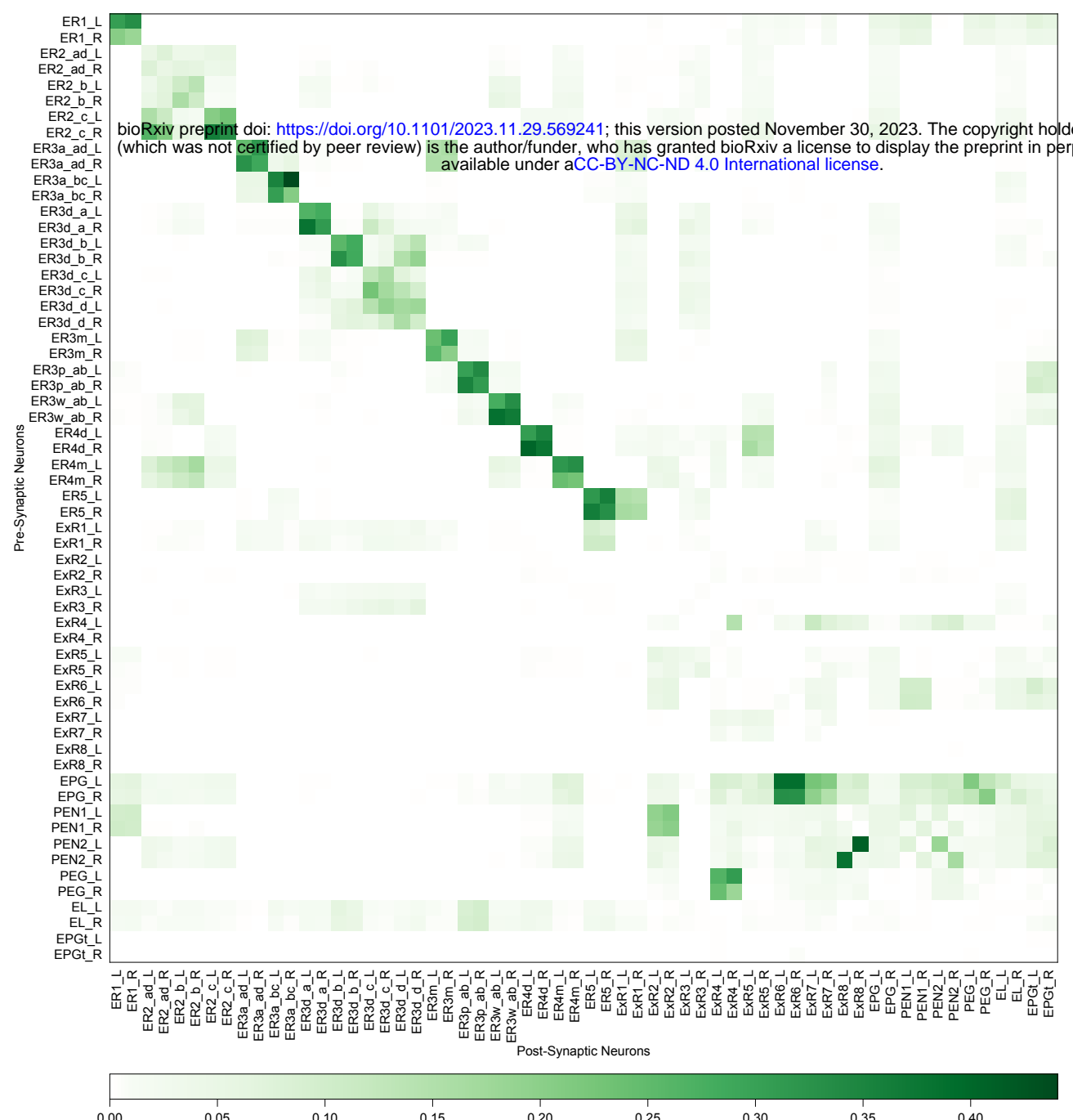


Fig. S7 | Synaptic Connections Between Ring and Columnar Neurons Within the Ellipsoid Body. Connection Matrix of various neuron types within the EB, including all visual ring neurons and lateral accessory lobe ring neurons [31, 61], extrinsic ring neurons [34], EPG neurons [1], PEN1 and PEN2 neurons [57, 101], and PEG, EL, and EPGt neurons [28, 29, 58, 102].